Downsizing of Three-Phase Wireless Power Transfer System with 12 coils by Reducing Magnetic Interference

Rintaro Kusui
Dept. of Electrical, Electronics, and Information Engineering
Nagaoka University of Technology
Nagaoka, Japan
kusui@stn.nagaokaut.ac.jp

Keisuke Kusaka
Dept. of Electrical, Electronics, and Information Engineering
Nagaoka University of Technology
Nagaoka, Japan
kusaka@vos.nagaokaut.ac.jp

Jun-ichi Itoh
Dept. of Electrical, Electronics, and Information Engineering
Nagaoka University of Technology
Nagaoka, Japan
itoh@vos.nagaokaut.ac.jp

Shuichi Obayashi
Corporate Research & Development Center
Toshiba Corporation
Kawasaki, Japan
shuichi.obayashi@toshiba.co.jp

Tetsu Shijo
Corporate Research & Development Center
Toshiba Corporation
Kawasaki, Japan
testu.shijo@toshiba.co.jp

Masaaki Ishida
Corporate Research & Development Center
Toshiba Corporation
Kawasaki, Japan
masaaki1.ishida@toshiba.co.jp

***Abstract*—In this paper, the placement of 12 coils for a three-phase WPT system with low-radiation noise is proposed for a reduction of a coil area. Increasing the charging power of a wireless power transfer (WPT) system is required in order to improve user convenience. One of the problems caused by the transmission of large power in a WPT system is radiation noise from the transmission coils. The proposed three-phase WPT system with the 12 coils suppresses radiation emission and cancels out the magnetic interference caused by multiple coils. However, it is necessary to increase the radius of the 12 coils, which are circularly placed, to satisfy the cancellation conditions of the magnetic interference. The proposed placement of the 12 coils reduces a radius by rotating each pair of the primary coils and the secondary coils. Simultaneously, the magnetic interference is canceled out and the radiation noise is suppressed. First, the principle of the cancellation of magnetic interference and radiation noise reduction is explained with an electromagnetic field analysis. Then, the emission from the 22-kW prototype has been measured according to the CISPR11 in an anechoic chamber. The magnetic interference is canceled out and the radiation noise is suppressed as same as the conventional placement with a reduced area by 74.5% in comparison with the conventional method.**

Keywords— wireless power transfer, three-phase transmission, leakage magnetic flux

I. Introduction

The number of electric vehicles (EVs) has been increasing for reducing the emission of NOx gas. The travel distance of EVs is typically shorter than conventional vehicles, so users need to more frequently charge a battery. Because of this inconvenience, EVs are not still a substitute for conventional vehicles with gasoline or diesel engines. Wireless power transfer (WPT) systems are actively studied [1-6] from the expectation to improve the convenience of EV users. WPT transmits power without a cable, thus the user will start charging without a connection of a charging cable.

Focusing on the wired chargers, the charging power has been increasing due to the increase in on-board battery capacity. Therefore, wireless chargers are also required to increase charging power. However, one of the problems for increasing charging power is radiation noise. The radiation noise interferes with electronic equipment or radio communication, and may adversely affect human health. Therefore, the WPT system must comply with the regulations established in each region or country based on CISPR and ICNIRP. The leakage magnetic flux has been shielded using metals or magnetic materials [7-10]. In addition, a reactive shield that reduces EMF emission by additional short-circuit coils is proposed [11-13]. However, an eddy current or short current is generated on the shield or additional windings causing large losses. In [14], the reduction method of radiation noise using the spectrum spread has been proposed. By randomly changing the transmission frequency, the peak of radiation noise is suppressed. However, this method will not comply with the international standard of WPT for EVs, which will be published by ISO/IEC. In [15], a two-channel WPT system has been proposed. The two-channel WPT system has two primary coils and two secondary coils placed in order to cancel out the radiation noise. Nevertheless, the flux which transmits the power has interfered between two channels when the radiation emission is canceled. In [16-17], a three-phase WPT system with 12 coils has been proposed. The three-phase WPT reduces the radiation noise without magnetic interference between the multiple coils. The six solenoid coils circularly placed on the primary and secondary side to suppress the radiation noise and cancel out the magnetic interference. The magnetic interference is canceled out by adjusting the magnetic coupling between the each primary and secondary side coils. However, the radius is increased in order to satisfy the interference cancellation condition at the conventional opposite placement.

In this paper, the placement to satisfy the cancellation condition with a smaller radius of 12 coils is proposed. In the proposed placement, each pair of the primary and secondary coils are rotated in order to reduce the magnetic coupling among the each the primary and secondary coils because the direction of the flux causing the interference is changed by the rotation of coils. Therefore, the cancellation condition is satisfied with the reduced area of coils. In the rest of the paper, first, the magnetic interference cancellation condition of the three-phase WPT system is shown and the placement reducing 12 coils area is proposed. Next, magnetic interference and magnetic field emission are analyzed. Then, the radiation noise of a 22-kW prototype is measured in the anechoic chamber complied with CISPR 11.

II. THREE-PHASE WPT SYSTEM WITH 12 COILS

A. Circuit Configuration

Figure 1 shows the circuit configuration of the three-phase WPT system with 12 coils. The WPT system is based on a three-phase WPT system with the coils, which are connected in star-star connection on the primary side and the secondary side, respectively. The resonant capacitors are connected to the output of the inverter and the input of the rectifier on each phase in the series.

Figure 2 shows the connection of the transmission coils and the resonant capacitors. The pairs of coils on the common phase are connected in series in a differential connection and placed opposite. Due to the differential connection, the magnetic flux, which is generated by two coils connected in series, is canceled out at the measurement point far from the coils. The coils of each phase are placed every 120 degrees. However, the multiple coils cause magnetic interference such as M_{an}, M_{bn}, and M_{cn} among the primary side and secondary side, where n represents the primary side as 1 and the secondary side as 2. The magnetic interference causes power factor deterioration, due to unnecessary induced voltage that does not contribute to power transmission.

B. Cancellation of Magnetic Interference

The unnecessary induced voltage is canceled out by adjusting magnetic coupling among the coils on the primary side and the secondary side.

The induced voltage on 12 coils is expressed as

$$\begin{pmatrix} v_{u1A} \\ v_{u1B} \\ v_{v1A} \\ v_{v1B} \\ v_{w1A} \\ v_{w1B} \\ v_{u2A} \\ v_{u2B} \\ v_{v2A} \\ v_{v2B} \\ v_{w2A} \\ v_{w2B} \end{pmatrix} = \begin{pmatrix} L_{1Ys} & M_{c1} & M_{b1} & M_{a1} & M_{b1} & M_{a1} & M & 0 & 0 & 0 & 0 & 0 \\ M_{c1} & L_{1Ys} & M_{a1} & M_{b1} & M_{a1} & M_{b1} & 0 & M & 0 & 0 & 0 & 0 \\ M_{b1} & M_{a1} & L_{1Ys} & M_{c1} & M_{b1} & M_{a1} & 0 & 0 & M & 0 & 0 & 0 \\ M_{a1} & M_{a1} & M_{c1} & L_{1Ys} & M_{a1} & M_{a1} & 0 & 0 & 0 & M & 0 & 0 \\ M_{b1} & M_{a1} & M_{b1} & M_{a1} & L_{1Ys} & M_{c1} & 0 & 0 & 0 & 0 & M & 0 \\ M_{a1} & M_{b1} & M_{a1} & M_{b1} & M_{c1} & L_{1Ys} & 0 & 0 & 0 & 0 & 0 & M \\ M & 0 & 0 & 0 & 0 & 0 & L_{2Ys} & M_{c2} & M_{b2} & M_{a1} & M_{b2} & M_{a1} \\ 0 & M & 0 & 0 & 0 & 0 & M_{c2} & L_{2Ys} & M_{a1} & M_{b2} & M_{a1} & M_{b2} \\ 0 & 0 & M & 0 & 0 & 0 & M_{b2} & M_{a1} & L_{2Ys} & M_{c2} & M_{b2} & M_{a1} \\ 0 & 0 & 0 & M & 0 & 0 & M_{a1} & M_{b2} & M_{c2} & L_{2Ys} & M_{a1} & M_{b2} \\ 0 & 0 & 0 & 0 & M & 0 & M_{b2} & M_{a1} & M_{b2} & M_{a1} & L_{2Ys} & M_{c2} \\ 0 & 0 & 0 & 0 & 0 & M & M_{a1} & M_{b2} & M_{a1} & M_{b2} & M_{c2} & L_{2Ys} \end{pmatrix} \frac{d}{dt} \begin{pmatrix} i_{u1} \\ -i_{u1} \\ i_{v1} \\ -i_{v1} \\ i_{w1} \\ -i_{w1} \\ i_{u2} \\ -i_{u2} \\ i_{v2} \\ -i_{v2} \\ i_{w2} \\ -i_{w2} \end{pmatrix} \quad (1),$$

where x represents A or B. The L_{nYs} is the self-inductance of each coil, and M is the mutual inductance of the magnetic coupling that transmits power.

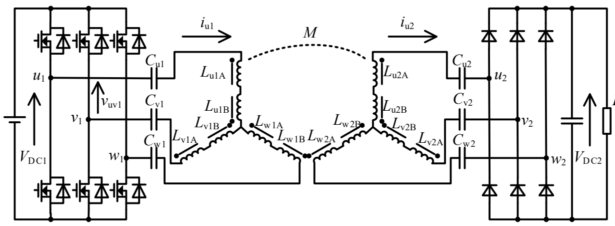

Fig. 1. Three-phase WPT system with 12 coils.

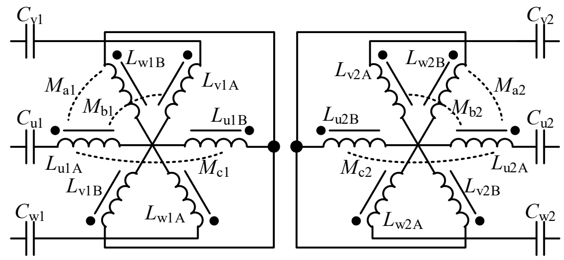

Fig. 2. Conection of the 12-coils and resonant capacitors.

Focusing on the first line of (1), the induced voltage on the coil L_{u1A} is expressed as

$$v_{u1A} = L_{1Ys}\frac{di_{u1}}{dt} + M\frac{di_{u2}}{dt} - M_{c1}\frac{di_{u1}}{dt} - M_{a1}\left(\frac{di_{v1}}{dt} + \frac{di_{w1}}{dt}\right) + M_{b1}\left(\frac{di_{v1}}{dt} + \frac{di_{w1}}{dt}\right) \quad (2).$$

The first term of (2) on the right side shows the induced voltage by self-inductance, and the second term shows the induced voltage by magnetic coupling between the primary coil and the secondary coil, which transmits power. By contrast, the third to fifth terms show unnecessary induced voltage by magnetic interference, which does not contribute to power transmission.

Assuming that the three-phase currents flowing through the coils are balanced, (2) is simplified as

$$v_{u1A} = L_{1Ys}\frac{di_{u1}}{dt} + M\frac{di_{u2}}{dt} - \omega I_{m1}\left(M_{c1}\cos\omega t + \left(M_{a1} - M_{b1}\right)\cos\left(\omega t - \frac{2}{3}\pi\right) + \left(M_{a1} - M_{b1}\right)\cos\left(\omega t - \frac{4}{3}\pi\right)\right) \quad (3),$$

where I_{m1} is the amplitude of the primary current.

The unnecessary induced voltage by the magnetic interference shown in (3) is canceled out when the relationship among the magnetic couplings M_{a1}, M_{b1}, and M_{c1} among the primary coils satisfy (4).

$$M_{a1} - M_{b1} - M_{c1} = 0 \quad (4)$$

The condition for cancellation magnetic interference is expressed as (5) using the coupling coefficient among the primary coils when the self-inductance of all primary coils is the same.

$$k_{a1} - k_{b1} - k_{c1} = 0 \tag{5}$$

The cancellation condition of the magnetic interference on the secondary side is derived as (6) in the same manner.

$$k_{a2} - k_{b2} - k_{c2} = 0 \tag{6}$$

By satisfying both (5) and (6), the unnecessary induced voltage due to the magnetic interference is canceled out. In other words, the three-phase WPT system with 12-coil is as same as the six independent single-phase WPT systems with two coils for each.

C. Proposed Placement of 12 coils

The cancellation conditions calculated by the equation (5) and (6) must be satisfied however the magnetic coupling k_a between adjacent coils is greatly larger than the magnetic coupling k_b and k_c because the distance between the adjacent coils is shorter than the other coils.

Figure 3 (a) shows top view of the conventional placement. In the conventional placement, the coils connected in series are placed in the face of each other. Therefore, in the conventional placement, the magnetic coupling between adjacent coils must be reduced by increasing the radius r of the 12 coils in order to satisfy (5) and (6).

Figure 3 (b) shows top view of the proposed 12 coils placement. In the proposed placement, the coils circularly placed are rotated around the center of each coil. Due to the rotation of each coil, the direction of the magnetic flux that interlinks across the same side coils and causes interference is changed. Thus, the unnecessary induced voltage is decreased. In other words, the magnetic coupling among the common side coils is reduced. Therefore (5) and (6) are satisfied even at smaller radius r.

The main magnetic coupling between the primary coil and the secondary coil that transmit the power does not significantly change because the coils are rotated for each pair of primary coils and secondary coils. Furthermore, the connection of the coils is not changed. Consequently, the transmission power and the reduction performance of radiation magnetic field is not significantly affected, when the coils are miniaturized by the proposed placement.

III. Electromagnetic Analysis

A. Analytical Model

In this section, the magnetic interference and radiation noise of a three-phase WPT system with the 12 coils are analyzed. The transmission coil cores of the analysis model have a length l of 500 mm, a width w of 250 mm, and a thickness h of 10 mm. The radius r indicates the distance from the center of the 12 coils to the center of each coil, and the coil rotation angle θ indicates the angle of rotation with the center of each coil. Table I shows parameters of the coils in the magnetic interference and radiation noise analysis.

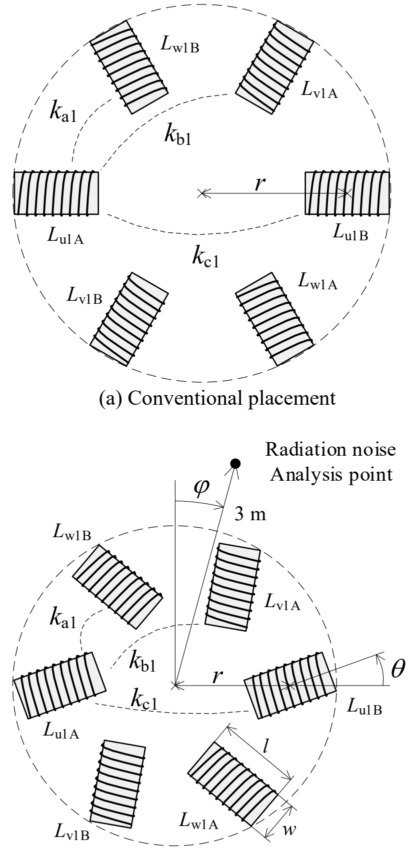

(b) Proposed placement

Fig. 3. Top view of 12 coils placement.

TABLE I. Specification of Prototype.

Prameters		Symbol	Value	
Rated power		P	22	kW
Primary voltage		V_{DC1}	650	V
Secondary voltage		V_{DC2}	200~400	V
Transmission frequency		f	85	kHz
Air gap		g	90	mm
Core width		w	250	mm
Core length		l	500	mm
Core thickness		h	10	mm
Number of turns	Primary	N_1	8	turn
	Secondary	N_2	5	turn
Self inductance	Primary	L_1	31.5	μH
	Secondary	L_2	12.8	μH
Core		PC95,TDK		
Litz wire		2UEWLZ 7×130(ϕ0.1)		
MOSFETs		BSM300A12P2E001, ROHM		
Diodes		IDW40G120C5BFKSA1, Infineon Technologies		
Litz wire		T_D	500	ns

B. *Magnetic Interference Analysis*

Figure 4 shows the analysis results of magnetic interference when the rotation angle θ is changed with a radius of 850 and 550 mm. The equation (5), (6) must be satisfied to cancel out the magnetic interference. The equation (5), (6) must be satisfied to cancel out the magnetic interference. When the value of $k_a - k_b - k_c$ is not zero, it is not canceled out. Then the value of $k_a - k_b - k_c$ means the infulence of magnetic interference. When the rotation angle θ is zero, the remaining interference of the 550-mm radius is three times larger than the 500-mm radius. This is the limitation for reducing the area of coils. From Fig. 4, it is shown that the remaining magnetic interference $k_a - k_b - k_c$ is reduced by rotating the coils by 40deg., i.e., the effect of magnetic interference is reduced. However, when the rotation angle is 40deg. or more, the effect of magnetic interference is increased. From this result, the radius is reduced from 850 to 550 mm with the same magnetic interference. Therefore, the area of the coils is reduced by 74.5%, with a rotation angle θ of 40deg and a smaller radius of 300 mm. Note that the minimum radius r is 500 mm because the core of the coil is 250 mm wide. However, in practice, there is an acrylic case that holds the cores and a winding. Due to this, in this paper, a radius of 550 mm is used in order to have a margin of 50 mm.

Figure 5 shows a vector diagram of the magnetic flux density when a current flows through only one coil. Fig. 5 (a) shows the magnetic flux without rotation of the coil. The magnetic flux is interlinked across the adjacent coil in the direction to generate the unnecessary induced voltage. The magnitude of the interlinkage flux that causes the induced voltage means the strength of the coupling. Therefore, when the coils are not rotated, the cancellation condition cannot be satisfied due to the strong coupling among the adjacent coils. On the other hand, from Fig. 5 (b), the magnetic flux interlinks across the adjacent coil from the side and flows to right and left when the coil is rotated by 40deg. For this reason, the magnetic coupling k_a between the adjacent coils is equivalently reduced, and the magnetic interference cancellation condition (5) and (6) is satisfied even when the radius is small. At other angles, the flux linkage branched to the left and right does not match, and magnetic coupling k_a is larger than when the rotation angle θ is 40deg. so that the magnetic interference is not sufficiently canceled out.

C. *Radiation Noise Analysis*

Figure 6 shows the electromagnetic analysis results of the fundamental wave component of the radiation noise. The radiation noise is analyzed at the radius r of 850 and 550 mm, and the coils rotation angle θ of 0 and 40 deg. The zero-rotation angle is the conventional placement and 40 deg. is the proposed placement. The radiation noise should be evaluated at 10 m from the system for a compatibility test of CISPR. However, this analysis is performed at 3 m from the center of the 12 coils in order to shorten the analysis time. The value θ indicates the angle at which the radiated magnetic field is analyzed. From Fig. 6, the average of the radiation noise is suppressed by 4.2 dBμA/m, by reducing the radius of the 12 coils. The distance between the same phase coils that connected differentially is shortened by reducing the radius. When the distance between the coils is short, the radiated noise is further reduced. As a result, the reduction effect is slightly improved when the radius r is reduced.

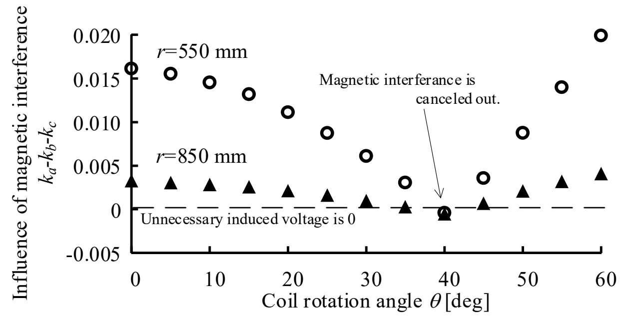

Fig. 4. Magnetic interference with changing rotation angle of coils.

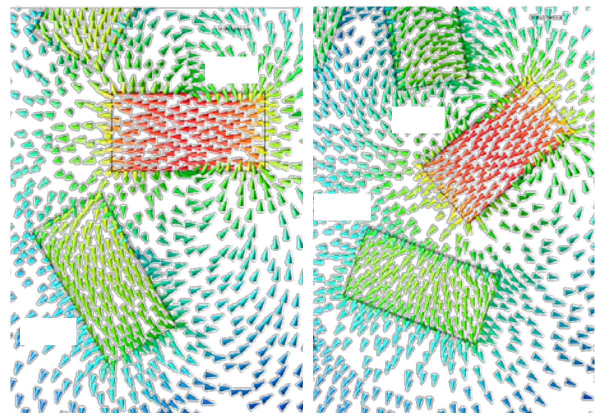

(a) Conventional placement (θ = 0deg.) (b) Proposed placement (θ = 40deg.)

Fig. 5. Vector diagram of magnetic flux density.

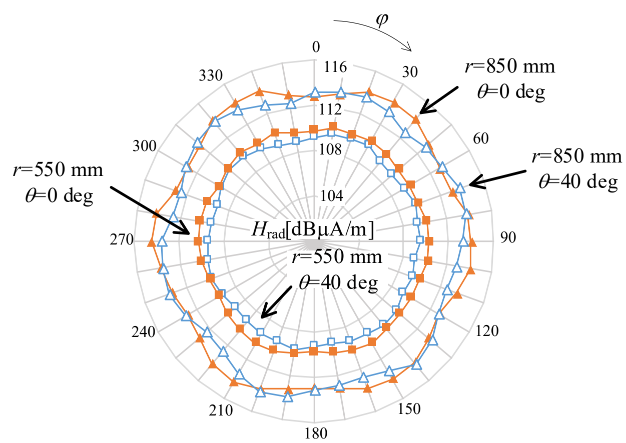

Fig. 6. Radiation noise analyzed by electromagnetic analysis.

IV. Evaluation of 22-Kw Prototype

A. *System configuration*

Figure 7 shows the configuration of a 22-kW prototype for a test. The input of the system is connected to a variable transformer so that the primary DC voltage is adjusted. The power is circulated from the output to the input of the WPT system by the bi-directional buck-boost chopper. Besides, the bi-directional buck-boost chopper adjusts the secondary DC

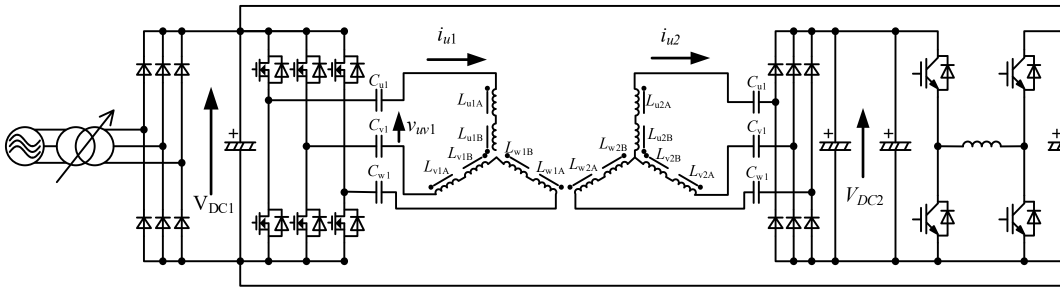

Fig. 7. System configuration of the 22-kW prototype.

voltage V_{DC2} from 200 to 400 V. The bi-directional buck-boost chopper emulates a constant voltage load such as a battery.

Figure 8 shows the transmission coil of the prototype. Fig. 8. (a) shows the conventional placement with a radius $r = 850$ mm and an angle $\theta = 0$ deg., and (b) shows the proposed placement with a radius $r = 550$ mm and an angle $\theta = 40$ degrees. The transmission coils have a ferrite core plate of 500 × 250 × 10 mm. The ferrite cores are put into an acrylic case. The winding used was a litz wire.

B. Operation Waveform

Figure 9 shows the operation waveforms of the three-phase WPT system when the 12 coils are placed with a radius $r = 550$ mm and rotation angle $\theta = 40$deg. The primary DC voltage V_{DC1} is 650 V, the secondary DC voltage V_{DC2} is 400 V, and the output power is 22 kW. The secondary DC voltage emulates the constant voltage load by the bi-direction buck-boost chopper. From Fig. 7, it is shown that the inverter output voltage is operating under the resonance condition because the rising and falling of the inverter output line-voltage are synchronized with the zero-cross of the inverter output current. Therefore, it is seen that the unnecessary induced voltage, that deteriorates the power factor, does not occur. In other words, the three-phase WPT system sufficiently canceled out the magnetic interference when the proposed placement is applied.

C. Radiation Noise Evaluation

Figure 10 shows the radiation noise measured according to CISPR 11, class A, group 2 in the anechoic chamber in Niigata, Japan. Note that the broken line from 150 kHz to 30 MHz in Fig. 10 indicates the regulation in the magnetic emission regulated by CISPR 11, class A, group 2. The regulation below 150 kHz has not been regulated in CISPR 11 edition 6.2, so far. Fig. 10 (a) shows the result for the conventional placement in which the radius r is 850 mm and the coil is not rotated. Fig. 10 (b) shows the result for the proposed placement in which the radius r is 550 mm and the rotation angle θ is 40 deg. From Fig. 10, it is shown that the three-phase WPT system with 12 coils sufficiently satisfies the regulation regulated from 150 kHz or more in both the conventional placement and the proposed placement. Focusing on the fundamental frequency component, the radiation noise is suppressed from 74.9 to 73.5 dBμA/m by the proposed placement. The proposed configuration of coils achieves the reduction of the coil area by 74.5% without degradation of the performance of radiation noise reduction.

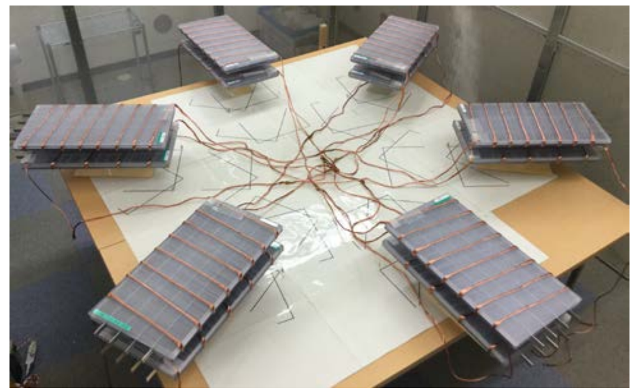

(a) conventional placement ($r = 850$ mm $\theta = 0°$)

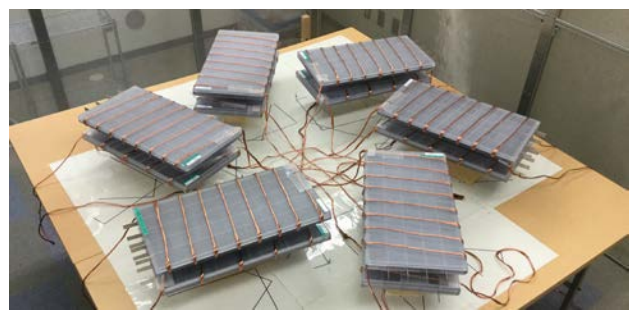

(b) proposed placement ($r = 550$ mm $\theta = 40°$)

Fig. 8. Transmission coils for 22-kW prototype.

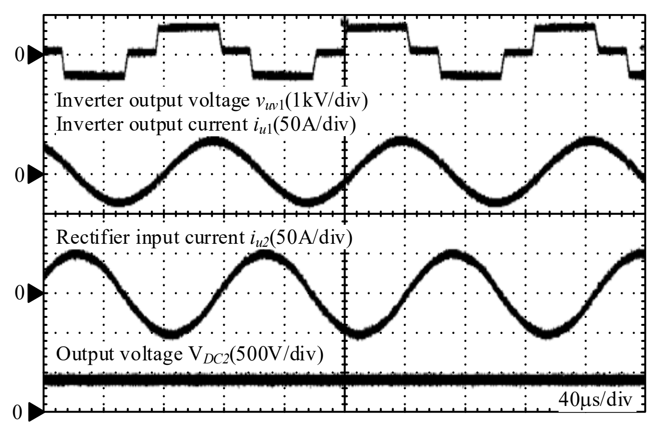

Fig. 9. Operation waveform.

V. Conclusion

The placement for miniaturizing a three-phase WPT system with 12 coils is proposed in this paper. The system has six

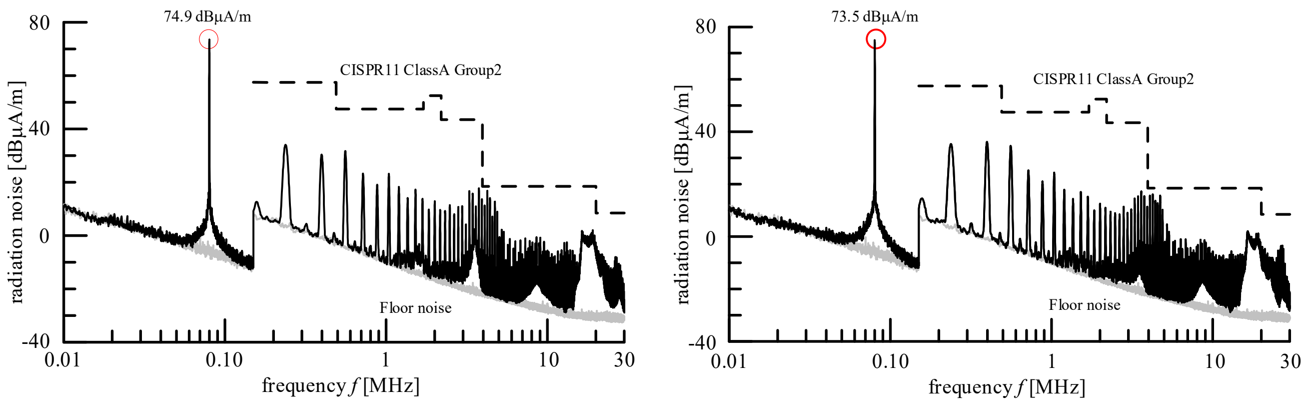

(a) conventional placement (r =850 mm θ=0°) (b) proposed placement (r =550 mm θ=40°)

Fig. 10. Radiation noise at 10 m from coil edge in anechoic chamber.

primary coils and six secondary coils placed circularly. Due to this, the magnetic interference is canceled out and the radiation noise is suppressed at the measurement point of the emission. The cancellation condition must satisfy $k_{an} - k_{bn} - k_{cn} = 0$ for the cancellation of the magnetic interference among the coils. The proposed placement satisfies the cancelation condition with a smaller radius of coils because the magnetic coupling between the adjacent coils is reduced by the rotation of each coil. The remaining magnetic interference $k_{an} - k_{bn} - k_{cn}$ and the magnetic flux density at 3 m from the center of 12 colils are analyzed by electromagnetic analysis. As the analysis result, the interference is canceled out when the coil rotation angle is 40deg. By canceling the interference, the area of the coils is reduced by 74.5%. Then, the emission of the 22-kW prototype with or without the proposed configuration of the coils is evaluated with complying with CISPR 11. The radiation noise is suppressed from 74.9 to 73.5 dBμA/m at the fundamental frequency and the magnetic interference is canceled out. The results show that the proposed configuration achieves both the reduction in the size of coils and radiation noise at the fundamental frequency.

In future work, the system efficiency and the suppression of radiation noise will be improved by optimizing the design of coils.

Acknowledgment

This research is financially supported by the Ministry of Internal Affairs and Communications of Japan.

References

[1] S. Li, C. C. Mi, “Wireless Power Transfer for Electric Vehicle Applications,” IEEE Journal of Emerging and Selected Topics in Power Electronics, Vol. 3, No. 1, pp. 4-17 (2015)

[2] R. Ota, N. Hoshi, J. Haruna, “Design of Compensation Capacitor in S/P Topology of Inductive Power Transfer System with Buck or Boost Converter on Secondary Side,” IEEJ Trans. on Industry Applications, Vol. 4, No. 4, pp. 476-485 (2015)

[3] F. Musavi, M. Edington and W. Eberle, “Wireless power transfer: A survey of EV battery charging technologies,” 2012 IEEE Energy Conversion Congress and Exposition (ECCE), pp. 1804-1810 (2012)

[4] T. Koyama, K. Umetani, E. Hiraki, “Design Optimization Method for the Load Impedance to Maximize the Output Power in Dual Transmitting Resonator Wireless Power Transfer System,” IEEJ Trans. on Industry Applications, Vol. 7, No. 1, pp. 49-55 (2019)

[5] J. Deng, W. Li, T. D. Nguyen, S. Li and C. C. Mi, "Compact and Efficient Bipolar Coupler for Wireless Power Chargers: Design and Analysis," in IEEE Trans. on Power Electronics, Vol. 30, No. 11, pp. 6130-6140 (2015)

[6] J. M. Miller, O. C. Onar and M. Chinthavali, "Primary-Side Power Flow Control of Wireless Power Transfer for Electric Vehicle Charging," in IEEE Journal of Emerging and Selected Topics in Power Electronics, Vol. 3, No. 1, pp. 147-162 (2015)

[7] J. Shin et al., "Design and Implementation of Shaped Magnetic-Resonance-Based Wireless Power Transfer System for Roadway-Powered Moving Electric Vehicles," IEEE Tran. on Industrial Electronics, vol. 61, no. 3, pp. 1179-1192 (2019)

[8] M. Mohammad, E. T. Wodajo, S. Choi and M. E. Elbuluk, "Modeling and Design of Passive Shield to Limit EMF Emission and to Minimize Shield Loss in Unipolar Wireless Charging System for EV," in IEEE Trans. on Power Electronics, Vol. 34, No. 12, pp. 12235-12245 (2019)

[9] H. Kim, J. Cho, S. Ahn, J. Kim, J. Kim, “Suppression of Leakage Magnetic Field from a Wireless Power Transfer System using Ferrimagnetic Material and Metallic Shielding,” IEEE International Symposium on EMC, 978-1-4673-2061-0, pp.640-645 (2012)

[10] K. Maikawa, K. Imai, Y. Minagawa, M. Arimitsu, H. Iwao, “Magnetic Field Reduction Technology of Wireless Charging System,” Society of Automotive Engineers of Japan 2013, No. 110-13 (2013)

[11] A. Tejeda, C. Carretero, J. T. Boys and G. A. Covic, “Ferrite-Less Circular Pad With Controlled Flux Cancelation for EV Wireless Charging,” IEEE Trans. on Power Electronics, Vol. 32, No. 11, pp. 8349-8359, (2017)

[12] S. Y. Choi, B. W. Gu, S. W. Lee, W. Y. Lee, J. Huh and C. T. Rim, “Generalized Active EMF Cancel Methods for Wireless Electric Vehicles,” IEEE Trans. on Power Electronics, Vol. 29, No. 11, pp. 5770-5783, (2014)

[13] K. Furukawa, K. Kusaka, J. Itoh, “General Analytical Model of Inductance Variation by EMF-canceling Coil for Inductive Power Transfer System”, IEEJ Trans. on Industry Applications, Vol. 8, No. 4, p. 660-668, (2019)

[14] K. Inoue, K. Kusaka, J. Itoh, “Reduction in Radiation Noise Level for Inductive Power Transfer Systems Using Spread Spectrum Techniques,” IEEE Trans. on Power Electronics, Vol. 33, No. 4 pp. 3076-3085 (2017)

[15] T. Shijo, K. Ogawa, M. Suzuki, Y. Kanekiyo, M. Ishida, S. Obayashi, “EMI Reduction Technology in 85 kHz Band 44 kW Wireless Power Transfer System for Rapid Contactless Charging of Electric Bus”, IEEE Energy Conversion Congress & Expo 2016, No. EC-0641 (2016)

[16] K. Kusaka, K. Furukawa, J. Itoh, “Development of Three-Phase Wireless Power Transfer System with Reduced Radiation Noise,” IEEJ Trans. on Industry Applications, Vol. 8, No. 4, pp. 600-607 (2019)

[17] K. Kusaka, R. Kusui, J. Itoh, D. Sato, S. Obayashi, M. Ishida, “A 22 kW-85 kHz Three-phase Wireless Power Transfer System with 12 coils,” IEEE Energy Conversion Congress and Exposition (ECCE) 2019, pp. 3340- 3347 (2019)